PNAS
www.pnas.org

Supplementary Information for
Observation of Methanediol ($CH_2(OH)_2$) – The Simplest Geminal Diol

Cheng Zhu[1,2,#], N. Fabian Kleimeier[1,2,#], Andrew M. Turner[1,2], Santosh K. Singh[1,2], Ryan C. Fortenberry[3*], Ralf I. Kaiser[1,2*]

[1] Department of Chemistry, University of Hawaii at Manoa, 2545 McCarthy Mall, Honolulu, HI 96822 (USA).

[2] W. M. Keck Laboratory in Astrochemistry, University of Hawaii at Manoa, 2545 McCarthy Mall, Honolulu, HI 96822 (USA).

[3] Department of Chemistry & Biochemistry, University of Mississippi, Mississippi 38677 (USA).

[#] C. Z. and N. F. K. contributed equally to this work

*Corresponding authors: Ryan C. Fortenberry, Ralf I. Kaiser

Email: r410@olemiss.edu, ralfk@hawaii.edu.

This PDF file includes:

Supplementary Information Text

Experimental. The experiments were performed at the W. M. Keck Research Laboratory in Astrochemistry (1-3). The experimental setup consists of a contamination-free stainless steel ultra-high vacuum chamber (UHV) evacuated to a base pressure of a few 10^{-11} Torr by magnetically levitated turbo molecular pumps coupled to oil-free scroll backing pumps. Within the chamber, a silver mirror substrate is interfaced to a cold finger, which is connected to a closed cycle helium compressor (Sumitomo Heavy Industries, RDK-415E). By utilizing a doubly differentially pumped rotational feedthrough (Thermionics Vacuum Products, RNN-600/FA/ MCO) and an UHV compatible bellow (McAllister, BLT106), the substrate is able to be rotated in the horizontal plane and to be translated vertically, respectively. The temperature of the silver wafer was monitored by a silicon diode sensor (Lakeshore DT-470) and regulated in a range of 5 to 300 K with a precision of ± 0.1 K by a programmable temperature controller (Lakeshore 336). After the wafer reached 5.0 ± 0.1 K, methanol (CH_3OH, Sigma-Aldrich, HPLC grade) and oxygen molecule (O_2, BOC Gases, Grade 5.0) (*SI Appendix*, Table S1) were co-deposited onto it via two glass capillary arrays to form an ice with a $CH_3OH : O_2 = (0.7 \pm 0.2) : 1$ composition ratio. Separate experiments with isotopically labeled ^{13}C-methanol ($^{13}CH_3OH$, Sigma-Aldrich, 99% ^{13}C atom), D_4-methanol (CD_3OD, Sigma-Aldrich, 99.8% D atom), ^{18}O-methanol ($CH_3{}^{18}OH$, Sigma-Aldrich, 95% O atom), and ^{18}O-oxygen ($^{18}O_2$, Cambridge Isotope Laboratories Inc., 97% O atom) were also conducted to observe infrared absorption and mass shifts of the products. The overall thickness of the ice was determined using laser interferometry (4) with one helium-neon laser (CVI Melles Griot; 25-LHP-230) operating at 632.8 nm. The laser light was reflected at an angle of 2° relative to the ice surface normal. Considering the refractive indexes of pure ices $n_{CH3OH} = 1.33 \pm 0.04$ and $n_{O2} = 1.25$ (5, 6), the ice thickness was calculated to be 500 ± 30 nm.

Mid-infrared (6,000 to 400 cm^{-1}) spectra of the ices were recorded utilizing a Nicolet 6700 Fourier transform infrared (FTIR) spectrometer with 4 cm^{-1} spectral resolution (*SI Appendix*, Figs. S1 and S2). The FTIR spectra of the pristine ice is shown in *SI Appendix*, Fig. S1. Detailed assignments of the peaks are compiled in *SI Appendix*, Table S2 (6-9). The ice composition was determined via a modified Beer-Lambert law (10). The average column density of CH_3OH was calculated to be $(4.9 \pm 0.9) \times 10^{17}$ molecules cm^{-2} based on the integrated areas along with absorption coefficients of 1.29×10^{-18} cm molecule^{-1} and 1.07×10^{-17} cm molecule^{-1} for the 1128 cm^{-1} (ν_{11}) and 1030 cm^{-1} (ν_8) bands, respectively (6). With the densities of CH_3OH ice (1.01 ± 0.03 g cm^{-3}) (6), its thickness was found to be 260 ± 50 nm. Considering the thickness of the total ice (500 ± 30 nm) and CH_3OH ice (260 ± 50 nm), the thickness of O_2 was estimated to be 240 ± 60 nm, which corresponds to a column density of $(6.8 \pm 1.5) \times 10^{17}$ molecules cm^{-2} taking into account the densities of O_2 ice (1.5 g cm^{-3}) (11). Therefore, the ratio of CH_3OH and O_2 was found to be (0.7 ± 0.2) : 1.

The ices were then isothermally irradiated at 5.0 ± 0.1 K with 5 keV electrons (Specs EQ 22-35 electron source) at a 70° angle to the ice surface normal for 30 min at currents of 0 nA (blank) and 50 nA (*SI Appendix*, Table S1). Using Monte Carlo simulations (CASINO 2.42) (12), the average penetration depths of the electrons were calculated to be 230 ± 25 nm (*SI Appendix*, Table S3), which is less than the 500 ± 30 nm ice thickness ensuring no interaction between the impinging electrons and the silver substrate. With the parameters compiled in *SI Appendix*, Table S3, the irradiation doses at 50 nA, 30 min were calculated to be 3.8 ± 0.6 eV per molecule. During the irradiation, in situ mid-infrared spectra of the ices were recorded every 2 minutes.

After the irradiation, the ices were heated to 300 K at a rate of 1 K min^{-1} (temperature programmed desorption (TPD)). During the TPD phase, any subliming molecules were detected using a reflectron time-of-flight (ReTOF) mass spectrometer (Jordon TOF Products, Inc.) with single photon ionization (1). This photoionization process utilizes distinct four wave mixing to produce vacuum ultraviolet light ($\omega_{vuv} = 2\omega_1 - \omega_2$) (*SI Appendix*, Table S4). The experiments were performed with 10.86 eV, 10.49 eV, 10.25 eV, and 9.50 eV photoionization energies to distinguish the CH_4O_2 isomers. The 10.49 eV light was generated via frequency tripling ($\omega_{vuv} = 3\omega_1$) of the third harmonic (355 nm) of the fundamental of a Nd:YAG laser (YAG A) in pulsed gas jets of Xe. To produce 10.86 eV, the second harmonic (532 nm) of a Nd:YAG laser was used to pump a Rhodamine 610/640 dye mixture (0.17/0.04 g L^{-1} ethanol) to obtain 606.948 nm (2.04 eV) (Sirah, Cobra-Stretch), which underwent a frequency tripling process to achieve ω_1 = 202.316 nm (6.13 eV) (β-BaB_2O_4 (BBO) crystals, 44° and 77°). A second Nd:YAG laser (second harmonic at 532 nm) pumped an LDS 867 (0.15 g L^{-1} ethanol) dye to obtain ω_2 = 888 nm (1.40 eV), which then combined with $2\omega_1$, using krypton as a non-linear medium, generated ω_{vuv} = 114.166 nm (10.86 eV) at 10^{12} photons per pulse. The production of 10.25 eV and 9.50 eV occurred similarly except the second harmonic (532 nm) and third harmonic (355 nm) of the second Nd:YAG laser were used to pump a Rhodamine 610/640 dye mixture (0.17/0.04 g L^{-1} ethanol) and a Coumarin 450 dye (0.40 g L^{-1} ethanol) to obtain ω_2 = 618 nm (2.01 eV) and ω_2 = 450 nm (2.76 eV), respectively. The VUV light was spatially separated from other wavelengths (due to multiple resonant and non-resonant processes ($2\omega_1 + \omega_2$; $3\omega_1$; $3\omega_2$)) using a lithium fluoride (LiF) biconvex lens (ISP Optics) and directed 2 mm above the sample to ionize subliming molecules. The ionized molecules were mass analyzed with the ReTOF mass spectrometer where the arrival time to a multichannel plate is based on mass-to-charge ratios, and the signal was amplified with a fast preamplifier (Ortec 9305) and recorded with a personal computer multichannel scalar (FAST ComTec, P7888-1 E), which is triggered via a pulse delay generator at 30 Hz. Here the ReTOF signal is the average of 3600 sweeps of the mass spectrum in 4 ns bin widths, which corresponds to an increase of the substrate temperature of 2 K.

Theoretical. The theoretical results are compile in *SI appendix*, Tables S5 to S8. The energies were computed using coupled cluster singles, doubles, and perturbative triples (CCSD(T)) method (13) with 2-point complete basis set (CBS) extrapolations (14) utilizing the aug-cc-pVTZ and aug-cc-pVQZ basis sets (15, 16) (*SI Appendix*,Tables S7 and S8). The CH_4O_2 structures were all optimized at the CCSD(T)/aug-cc-pVTZ level producing zero-point vibrational energies (ZPVEs). Adiabatic ionization energies were determined from the CCSD(T)/CBS + ZPVE energy difference between the optimized neutral and cation species. The CCSD(T) computations employed the Molpro 2015.1 quantum chemical program (17, 18). The computation error range of the ionization energies extracted at this level of theory was determined to be −0.05 eV to + 0.03 eV by comparing the experimental and computed ionization energies of different carbon-, hydrogen-, and oxygen-containing compounds (*SI Appendix*,Tables S6 and S7). The electric field of the ReTOF extractor plate lowers the ionization energies by 0.03 eV (*SI Appendix*, Tables S6 and S7) (19). The vibrational frequencies for all CH4O2 isomers/conformers and isotopically labelled species (18O, 13C, and D) were also computed at the CCSD(T)-F12b/cc-pVTZ-F12 level of theory (*SI Appendix*, Table S5).

It is interesting to recall that in case of the neutrals, both methanediol ($CH_2(OH)_2$) conformers **1'** and **1''** are lower in energy compared to the water – formaldehyde complex (H_2O-H_2CO) **2** by 21 and 11 kJ mol^{-1}, respectively (Figure 3). However, in case of the cations, the ionized water – formaldehyde complex (H_2O-H_2CO^+) $\mathbf{2^+}$ is lower in energy compared to the cations of methanediol ($CH_2(OH)_2$ conformers $\mathbf{1'^+}$ and $\mathbf{1''^+}$ by 11 and 35 kJ mol^{-1}, respectively. Nevertheless, as revealed via a normal coordinate analysis, all three cations are stable and minima (Table S5). In $\mathbf{2^+}$, the complex is actually twisted with the water out of the plane of the formaldehyde; the neutral complex **2** is planar.

Ionization thresholds of formaldehyde···water complex and methanediol. To experimentally determine the ionization threshold of the formaldehyde (H_2CO) ··· water (H_2O) complex (**3**), we deposited H_2CO-H_2O ices, exploited PI-ReTOF to monitor the subliming molecules and complexes during TPD of the ices, and repeated the experiments in a photon energy (PE) range of 10.40 eV to 10.49 eV (*SI Appendix*, Figs. S3 and S4). The H_2CO-H_2O ices were prepared by co-depositing the formaldehyde monomer obtained by heating paraformaldehyde (Sigma Aldrich) (20) at 333 K and water vapor via two separate glass capillary arrays with a ratio of H_2CO : H_2O = 1:10. For the TPD profile of *m/z* = 48 (PE = 10.49 eV), a sublimation event at 170 K was detected (*SI Appendix*, Fig. S3). The signal disappears at PE < 10.44 ± 0.01 eV (*SI Appendix*, Fig. S4). The ionization threshold 10.44 ± 0.01 eV falls well into the computed IE range of **3** (10.37 - 10.45 eV).

To experimentally determine the ionization threshold of the carrier of the sublimation events at 181 K (Fig. 3(a)), we repeated the irradiation and TPD experiments of CH_3OH-O_2 ices in a photon energy (PE) range of 10.63 eV to 10.82 eV (*SI Appendix*, Fig. S5). The results show that the *m/z* = 48 signal in the 181 K region appears at PE = 10.73 ± 0.01 eV, which indicates the carrier of the 181 K peak has an ionization energy of 10.73 ± 0.01 eV; this sublimation event can only be assigned to C_2 - methanediol ($CH_2(OH)_2$,**1'**) (computed IE = 10.66 - 10.74 eV). Conformer **1'** is thermodynamically more stable than C_s - methanediol ($CH_2(OH)_2$,**1''**) by 10 kJ mol^{-1} (*SI Appendix*, Table S7). Under thermal equilibrium conditions at the sublimation temperatures of **1'** (about 180 K), the branching ratio of **1'** to **1''** can be determined to be about 800 with $e^{-\Delta_R G/RT}$ ($\Delta_R G$ is the difference between the standard Gibbs free energies of **1'** and **1''**, T is the temperature, and R is the ideal gas constant); this supports the absence of **1"** in our experiments.

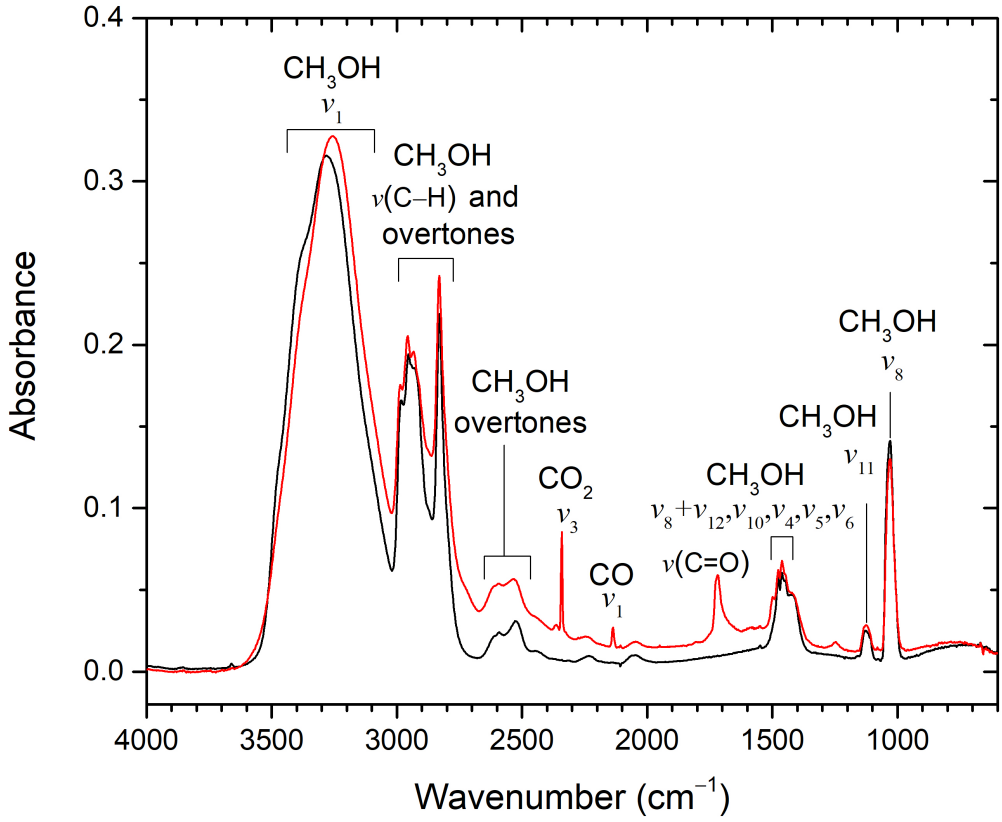

Fig. S1. FTIR spectra of the methanol (CH_3OH) and oxygen (O_2) ice mixture before (black) and after (red) processing with energetic electrons. For clarity, only significant peaks are labeled; detailed assignments are compiled in *SI Appendix*, Table S2.

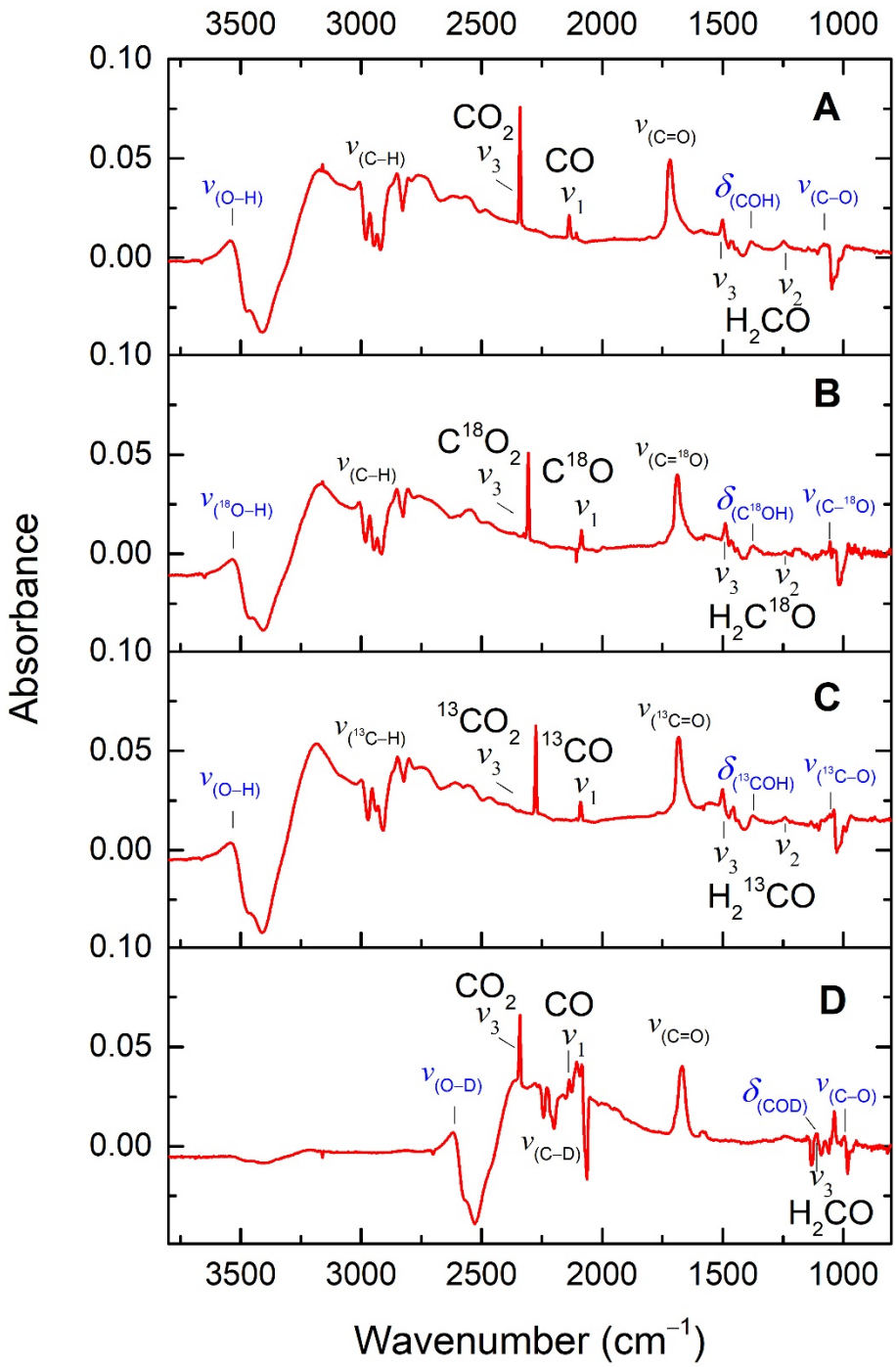

Fig. S2. Difference FTIR spectra of 5 keV electron processed and pristine ices. **A**, $CH_3OH + O_2$; **B**, $CH_3{}^{18}OH + {}^{18}O_2$; **C**, $^{13}CH_3OH + O_2$; **D**, $CD_3OD + O_2$; For clarity, only significant peaks are labeled; detailed assignments are compiled in *SI Appendix*, Table S2.

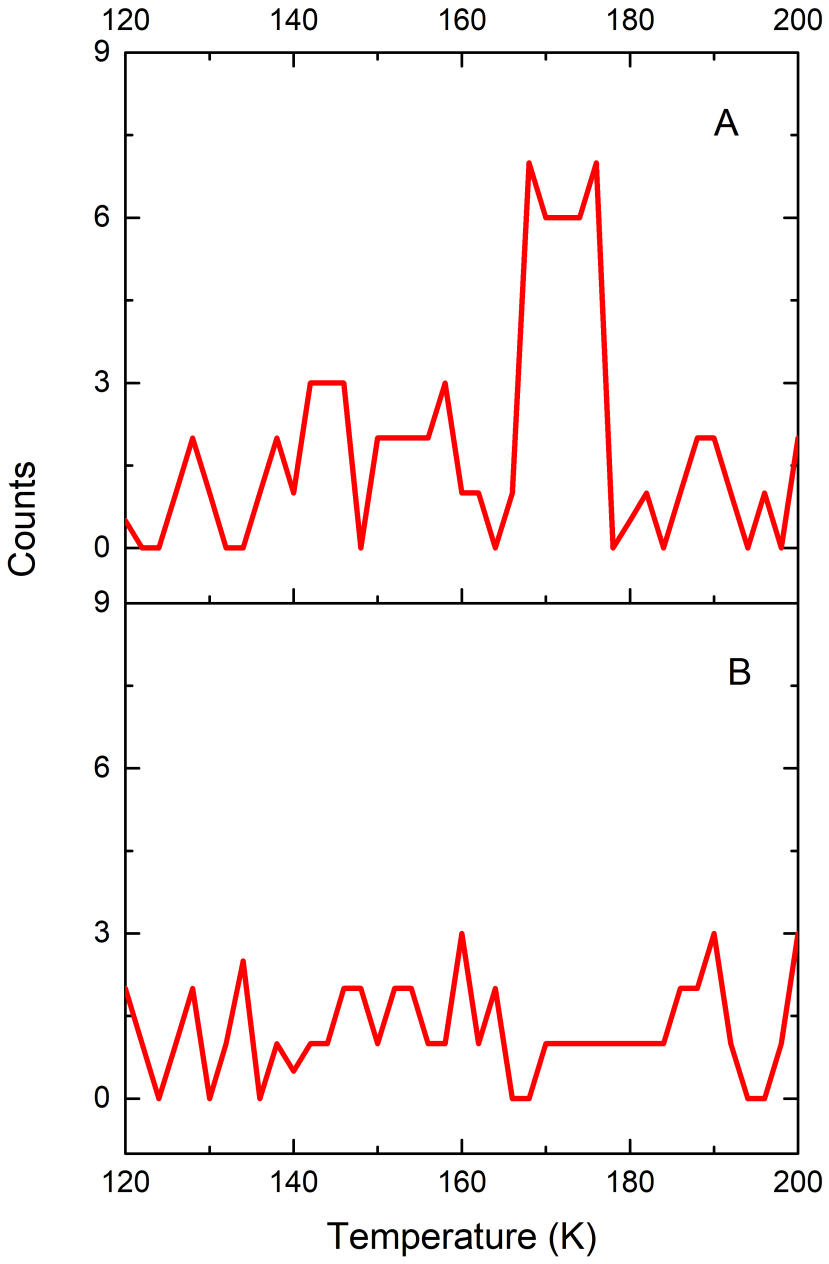

Fig. S3. PI-ReTOF-MS data at *m/z* = 48 during the TPD phase of fromaldehyde (H_2CO) and water (H_2O) ice mixtures. **A**, PE = 10.49 eV; **B**, PE = 10.40 eV. The peak at 170 K is associated with the sublimation of the $H_2CO\cdots H_2O$ complex (**3**).

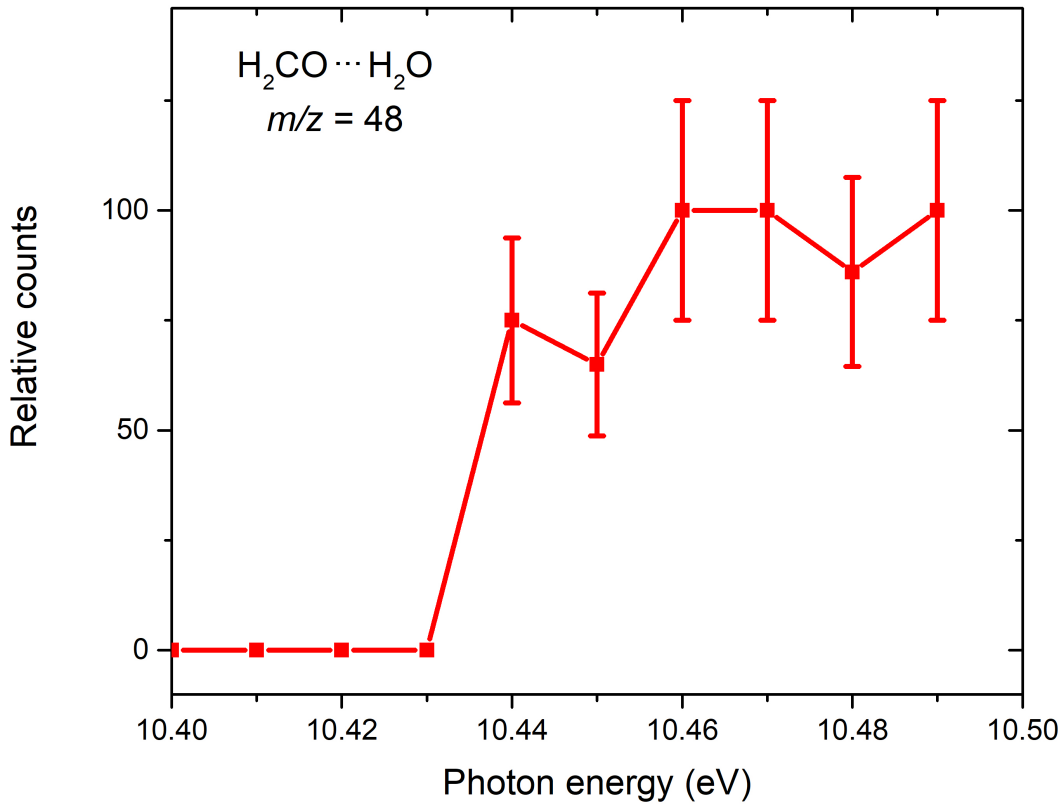

Fig. S4. Photoionization efficiency of the formaldehyde (H_2CO)···water (H_2O) complex (H_2CO···H_2O, **3**). The ionization threshold of **3** is 10.44 ± 0.01 eV.

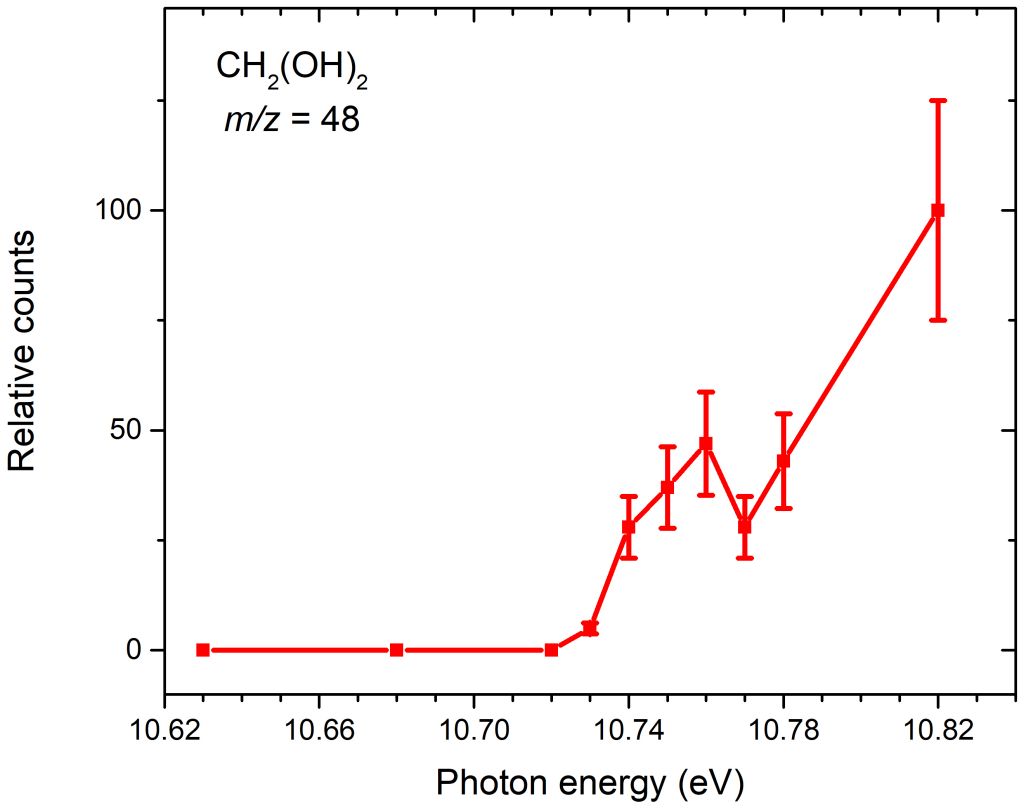

Fig. S5. Photoionization efficiency of methanediol ($CH_2(OH)_2$). The ionization threshold is 10.73 ± 0.01 eV.

Table S1. List of experiments

#	Precursors	Electron (nA)	Irradiation time (min)	Photoionization energy (eV)
1	$CH_3OH + O_2$	0 (blank)	0	10.86
2	$CH_3OH + O_2$	50	30	10.86
3	$CH_3OH + O_2$	50	30	10.49
4	$CH_3OH + O_2$	50	30	10.25
5	$CH_3OH + O_2$	50	30	9.50
6	$CH_3{}^{18}OH + {}^{18}O_2$	50	30	10.86
7	$^{13}CH_3OH + O_2$	50	30	10.86
8	$CD_3OD + O_2$	50	30	10.86

Table S2. Infrared absorption peaks before and after irradiation for methanol and oxygen ice mixture[a]

Pristine ice, before irradiation (5 K)				
$CH_3OH + O_2$	$CH_3{}^{18}OH + O_2$	$^{13}CH_3OH + O_2$	$CD_3OD + O_2$	Assignment
3280	3272	3281	2440	CH_3OH (ν_1)
2985	2985	2973	2246	CH_3OH (ν_2)
2955	2954	2950	2216	CH_3OH (ν_9)
2926	2926	2919	2151	CH_3OH ($\nu_4 + \nu_5/\nu_4 + \nu_{10}/\nu_5 + \nu_{10}/2\nu_4/2\nu_{10}/2\nu_5$)
2830	2830	2825	2073	CH_3OH ($\nu_3/2\nu_6$)
2593	2593	2587	2012	CH_3OH ($\nu_4 + \nu_{11}/\nu_7 + \nu_4/\nu_6/\nu_{10}$)
2525	2522	2515	-	CH_3OH ($\nu_6 + \nu_{11}$)
2436	2415	2416	-	CH_3OH ($\nu_6 + \nu_8$)
2238	2230	2221	1938	CH_3OH ($2\nu_{11}/2\nu_7$)
2043	2005	2011	1661	CH_3OH ($2\nu_8$)
1476	1476	1475	1126	CH_3OH (ν_4)
1462	1461	1460	1116	CH_3OH (ν_{10})
1449	1447	1443	1095	CH_3OH (ν_5)
1420	1419	1416	1063	CH_3OH (ν_6)
1128	1126	1118	900	CH_3OH (ν_{11})
1030	1005	1010	833	CH_3OH (ν_8)
New peaks after irradiation (5 K)				
3550	3531	3540	2615	OH
2976	2970	2952	2219	CH
2341	2308	2276	2341	CO_2 (ν_3)
2137	2088	2090	2138	CO (ν_1)
1720	1677	1683	1699, 1670	C=O stretch
1500	1496	1499	1112	H_2CO (ν_3) ?
1378	1370	1371	1112	δ_{C-O-H} ?
1249	1243	1241	-	H_2CO (ν_2)
1075	1055	1051	995	ν_{C-O}

Note.

[a] References: Bouilloud et al. (2015) (6), Socrates (2004) (7), Maity et al. (2015) (8), Zhu et al. (2020) (9).

Table S3. Data applied to calculate the average irradiation dose per molecule

Initial kinetic energy of the electrons, E_{init} (keV)	5
Ice	$CH_3OH + O_2$
Irradiation current, I (nA)	50 ± 5
Total number of electrons	$(5.6 \pm 0.6) \times 10^{14}$
Average penetration depth, l_{ave} (nm)[a]	230 ± 25
Average kinetic energy of backscattered electrons, E_{bs} (keV)[a]	3.35 ± 0.34
Fraction of backscattered electrons, f_{bs}[a]	0.36 ± 0.04
Average kinetic energy of transmitted electrons, E_{trans} (keV)[a]	0
Fraction of transmitted electrons, f_{trans}[a]	0
Irradiated area, A (cm^2)	1.0 ± 0.1
Dose (eV/molecule)	3.8 ± 0.6

Note.
[a] Parameters obtained from CASINO software v2.42.

Table S4. Parameters for the generation of vacuum ultraviolet (VUV) light used in the present experiments[a]

$2\,\omega_1 - \omega_2$	Photoionization energy (eV)	10.86	10.49 ($3\omega_1$)	10.25	9.50
	Flux (10^{11} photons s^{-1})	10 ± 1	12 ± 1	10 ± 1	10 ± 1
	Wavelength (nm)	114.166	118.193	120.960	130.510
ω_1	Wavelength (nm)	202.316	355	202.316	202.316
Nd:YAG (YAG A)	Wavelength (nm)	532	355	532	532
Dye laser (DYE A)	Wavelength (nm)	606.948	-	606.948	606.948
Dye		Rhodamine 610+640	-	Rhodamine 610+640	Rhodamine 610+ 640
ω_2	Wavelength (nm)	888	-	618	450
Nd:YAG (YAG B)	Wavelength (nm)	532	-	532	355
Dye laser (DYE B)	Wavelength (nm)	888	-	618	450
Dye		LDS 867	-	Rhodamine 610+640	Coumarin 450
	Nonlinear medium	Kr	Xe	Kr	Kr

Note.
[a] The uncertainty for VUV photon energies is 0.01 eV.

Table S5 Computed vibrational frequencies for all CH_4O_2 isomers/conformers and isotopically labelled species (^{18}O, ^{13}C, and D) at the CCSD(T)-F12b/cc-pVTZ-F12 level of theory

1' (*C*$_2$-$CH_2(OH)_2$)			**1''** (*C*s- $CH_2(OH)_2$)			**2** (CH_3OOH)			**3** ($H_2CO\cdots H_2O$)		
Normal	Harmonic	Anharmonic	Normal	Harmonic	Anharmonic	Normal	Harmonic	Anharmonic	Normal	Harmonic	Anharmonic
ZPT	12663.6	12470.1	ZPT	12555.0	12345.2	ZPT	12047.0	11857.6	ZPT	11264.2	11133.0
1	3834.2	3646.2	1	3850.2	3662.9	1	3791.0	3596.8	1	3918.9	3726.4
2	3834.0	3646.5	2	3848.2	3660.5	2	3135.5	2981.0	2	3746.8	3591.1
3	3110.5	2974.7	3	3148.9	2989.3	3	3106.5	2963.4	3	3048.7	2888.7
4	3055.7	2922.9	4	3021.1	2884.8	4	3027.2	2917.3	4	2959.5	2801.6
5	1542.7	1501.7	5	1530.1	1492.1	5	1519.8	1476.2	5	1763.9	1733.5
6	1457.7	1410.9	6	1448.9	1411.7	6	1477.1	1432.6	6	1666.0	1613.8
7	1405.4	1355.0	7	1426.5	1366.4	7	1456.7	1421.7	7	1533.6	1496.9
8	1384.4	1336.5	8	1386.0	1338.0	8	1374.2	1348.2	8	1281.5	1257.7
9	1218.9	1191.3	9	1177.0	1137.7	9	1214.0	1182.7	9	1200.1	1179.0
10	1096.1	1060.4	10	1090.1	1053.8	10	1180.6	1156.2	10	502.7	424.5
11	1055.4	1027.6	11	1078.0	1051.1	11	1059.0	1026.3	11	368.9	297.5
12	1019.2	1007.2	12	1007.6	995.9	12	860.4	831.4	12	191.3	138.4
13	565.1	543.7	13	543.8	534.1	13	449.6	440.4	13	178.8	178.8
14	378.9	366.5	14	382.3	333.1	14	257.0	249.6	14	115.2	49.8
15	369.0	332.8	15	171.2	126.4	15	185.4	94.2	15	52.5	405.4
^{18}O	Harmonic	Anharmonic	^{18}O	Harmonic	Anharmonic	^{18}O	Harmonic	Anharmonic	^{18}O	Harmonic	Anharmonic
ZPT	12601.3	12409.1	ZPT	12493.5	12285.3	ZPT	11984.3	11796.5	ZPT	11215.8	11080.5
1	3821.9	3634.9	1	3837.6	3651.4	1	3778.2	3585.3	1	3904.5	3713.6
2	3821.6	3635.2	2	3835.7	3649.1	2	3135.5	2981.0	2	3737.2	3582.4
3	3110.5	2973.2	3	3148.9	2989.1	3	3106.5	2963.1	3	3048.7	2885.7
4	3055.7	2922.6	4	3021.1	2883.2	4	3027.2	2915.7	4	2959.5	2801.2
5	1542.7	1501.3	5	1530.0	1492.5	5	1519.5	1478.4	5	1731.0	1700.1

6	1455.1	1422.1	6	1447.3	1410.1	6	1476.9	1431.6	6	1659.6	1607.6
7	1399.0	1342.9	7	1418.6	1387.2	7	1456.5	1419.8	7	1521.8	1487.0
8	1377.5	1350.7	8	1380.5	1330.9	8	1365.4	1338.5	8	1276.2	1252.6
9	1217.1	1189.2	9	1175.7	1132.3	9	1204.0	1173.0	9	1198.7	1177.6
10	1071.7	1037.4	10	1065.9	1031.2	10	1177.5	1153.0	10	501.5	423.6
11	1024.8	998.5	11	1057.1	1037.0	11	1028.8	998.6	11	367.3	296.4
12	1018.8	1006.1	12	998.1	983.5	12	818.0	790.7	12	181.9	133.2
13	542.6	520.9	13	518.7	511.0	13	435.6	427.9	13	178.7	178.7
14	377.1	365.7	14	381.3	332.6	14	254.4	247.2	14	112.8	50.0
15	366.4	330.8	15	170.4	126.3	15	184.5	93.9	15	52.2	402.0
^{13}C	Harmonic	Anharmonic	^{13}C	Harmonic	Anharmonic	^{13}C	Harmonic	Anharmonic	^{13}C	Harmonic	Anharmonic
ZPT	12616.8	12424.5	ZPT	12508.1	12299.8	ZPT	12007.4	11819.1	ZPT	11224.0	11093.6
1	3834.2	3646.2	1	3850.2	3662.9	1	3791.0	3596.8	1	3918.9	3726.4
2	3834.0	3646.5	2	3848.2	3660.5	2	3124.0	2971.0	2	3746.8	3591.1
3	3098.0	2962.5	3	3138.0	2979.8	3	3094.9	2953.3	3	3035.6	2880.6
4	3050.1	2915.4	4	3013.9	2871.1	4	3024.5	2910.1	4	2955.0	2797.4
5	1537.8	1497.2	5	1525.2	1487.7	5	1517.3	1471.5	5	1725.6	1696.4
6	1451.0	1419.0	6	1444.0	1407.1	6	1474.8	1430.0	6	1665.7	1613.8
7	1403.2	1348.4	7	1415.4	1383.9	7	1449.5	1415.2	7	1533.3	1497.0
8	1374.0	1325.9	8	1384.9	1335.5	8	1373.5	1345.5	8	1272.0	1248.2
9	1214.4	1187.5	9	1176.4	1132.1	9	1202.8	1172.1	9	1187.9	1167.3
10	1072.8	1038.3	10	1065.6	1031.6	10	1172.6	1148.4	10	502.7	424.4
11	1040.9	1013.6	11	1058.7	1033.7	11	1044.1	1011.5	11	368.5	297.4
12	1013.4	1001.5	12	1002.0	990.0	12	857.6	829.1	12	191.3	138.4
13	563.0	541.4	13	540.8	531.4	13	445.8	437.0	13	178.8	178.8
14	378.2	366.1	14	381.7	332.8	14	257.0	249.6	14	113.5	50.0
15	368.5	332.4	15	171.2	126.4	15	185.3	94.0	15	52.4	405.1

D	Harmonic	Anharmonic	D	Harmonic	Anharmonic	D	Harmonic	Anharmonic	D	Harmonic	Anharmonic
ZPT	9669.9	9560.3	ZPT	9587.0	9474.1	ZPT	9178.1	9073.0	ZPT	8556.7	8480.8
1	2790.9	2692.2	1	2803.5	2704.8	1	2761.9	2659.1	1	2865.1	2759.7
2	2790.6	2691.7	2	2802.0	2703.0	2	2326.2	2245.8	2	2708.6	2627.1
3	2319.3	2262.1	3	2338.2	2264.8	3	2305.9	2227.6	3	2277.8	2188.8
4	2218.5	2083.7	4	2202.3	2087.4	4	2167.2	2062.6	4	2156.1	2075.2
5	1180.5	1158.7	5	1171.6	1146.3	5	1168.9	1135.4	5	1714.2	1688.1
6	1169.3	1135.7	6	1150.8	1120.9	6	1090.4	1063.9	6	1216.1	1189.5
7	1114.8	1089.9	7	1132.5	1107.9	7	1068.7	1044.7	7	1119.4	1098.2
8	1046.5	1072.2	8	1022.3	996.0	8	1060.9	1038.8	8	1009.6	996.2
9	1006.6	983.2	9	1008.2	989.8	9	991.0	958.5	9	960.7	947.2
10	1002.4	981.5	10	1006.1	985.8	10	968.9	941.9	10	363.1	316.9
11	870.0	855.0	11	843.9	833.3	11	904.5	889.6	11	274.1	234.4
12	753.9	735.6	12	764.8	771.5	12	804.9	783.6	12	179.4	136.9
13	522.6	508.6	13	523.1	509.2	13	404.7	402.9	13	127.6	127.6
14	278.4	257.2	14	278.8	251.8	14	195.7	190.8	14	102.5	55.2
15	275.4	266.2	15	125.9	100.4	15	136.3	92.1	15	39.0	231.0

Table S6 Comparison of experimental to computed ionization energies (CCSD(T)/CBS//B3LYP/cc-pVTZ + zero-point vibrational energy (ZPVE) corrections) of different carbon-, hydrogen-, and oxygen- containing compounds with average deviations computed from the error limits. Combined error limits are used to obtain the corrected computed ionization energies.

Structure	Name	Experimental IE (eV)	References	Computed IE (eV)	Computed IE – Experimental IE (max) (eV)	Computed IE – Experimental IE (min) (eV)
	Acetone	9.703 ± 0.006	1	9.71	−0.001	−0.013
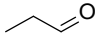	Propanal	9.96 ± 0.01	1	9.97	0.00	-0.02
	Propylene oxide	10.22 ± 0.02	2	10.24	0.00	−0.04
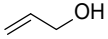	2-Propen-1-ol	9.67 ± 0.03	1	9.65	0.05	−0.01
	Methanol	10.84 ± 0.01	3	10.86	−0.01	−0.03
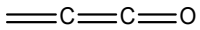	Propadienone	9.12 ± 0.05	3	9.15	0.02	−0.08
	Formaldehyde	10.88 ± 0.01	3	10.89	0.00	−0.02
	Ketene	9.617 ± 0.003	3	9.58	0.040	0.034
	Acetaldehyde	10.229 ± 0.0007	3	10.24	−0.0103	−0.0117
					Average 0.01 ± 0.02	Average −0.02 ± 0.03
					Error Limits –0.01 to +0.03	Error Limits –0.05 to +0.01
					Combined Error Limits –0.05 - +0.03	

Table S7. Calculated adiabatic ionization energies (IE) and relative energies ($E_{rel.}$) of distinct CH_4O_2 isomers and formaldehyde ··· water complex ($H_2CO\cdots H_2O$).

Structure	#	IE (eV)[a]	$E_{rel.}$ (kJ mol^{-1})[b]	Corrected IE after error analysis (eV)	Corrected IE with electric field effect (eV)
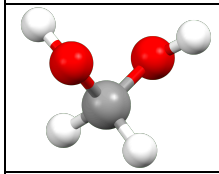	**1'** (C_2-Methanediol)	10.74	0	10.69 - 10.77	10.66 - 10.74
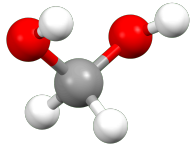	**1''** (C_s-Methanediol)	10.65	10	10.60 - 10.68	10.57 - 10.65
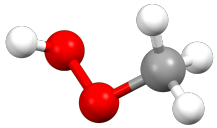	**2** (Methyl peroxide)	9.81	267	9.76 - 9.84	9.73 - 9.81
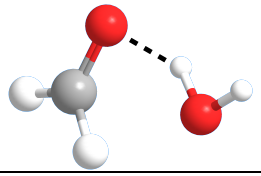	**3** ($H_2CO\cdots H_2O$ complex)	10.45	21	10.40 - 10.48	10.37 - 10.45

Notes.

[a] Adiabatic ionization energies by CCSD(T)/CBS with CCSD(T)/aug-cc-pVTZ zero point vibration energy (ZPVE) correction.

[b] Relative energies by CCSD(T)/CBS with CCSD(T)/aug-cc-pVTZ ZPVE correction.

Table S8. Computed Cartesian coordinates (Å) and vibrational frequencies (cm^{-1}) for CH_4O_2 isomers, formaldehyde ··· water complex ($H_2CO\cdots H_2O$), ions, and the transition state for unimolecular dehydration of $CH_2(OH)_2$.

1' (C_2-Methanediol)

C	0.0000000000	0.0000000000	0.5490095797
H	-0.0346511279	0.8949330727	1.1741112998
H	0.0346511279	-0.8949330727	1.1741112998
O	1.1705643047	-0.0477015485	-0.2325729844
O	-1.1705643047	0.0477015485	-0.2325729844
H	1.2028975015	0.7626112238	-0.7534997804
H	-1.2028975015	-0.7626112238	-0.7534997804

Frequencies	361.28	375.30	558.73	1012.42	1044.90
Frequencies	1086.67	1211.25	1377.80	1399.04	1451.41
Frequencies	1541.06	3051.09	3104.31	3811.83	3812.13

C_{2v}-Methanediol$^+$

C	0.0000000000	0.0000000000	0.4789388231
H	-0.0000954489	0.8501604610	1.2477683827
H	0.0000954489	-0.8501604610	1.2477683827
O	1.1007816513	-0.0000094760	-0.2749954575
O	-1.1007816513	0.0000094760	-0.2749954575
H	1.9136699936	0.0001289258	0.2637255758
H	-1.9136699936	-0.0001289258	0.2637255758

Frequencies	227.81	361.66	391.42	697.29	959.49
Frequencies	1102.09	1127.32	1219.14	1372.54	1387.10
Frequencies	1946.89	2421.56	2583.10	3678.74	3789.50

1'' (C_s-Methanediol)

C	0.5316812649	0.0573441740	0.0000000000
H	1.0754617777	1.0091440233	0.0000000000
H	1.2332235232	-0.7738144450	0.0000000000
O	-0.2282485848	-0.0760317532	-1.1792206255
O	-0.2282485848	-0.0760317532	1.1792206255
H	-0.6991284799	0.7475474207	-1.3407848339
H	-0.6991284799	0.7475474207	1.3407848339

Frequencies	163.96	376.53	537.26	1001.03	1067.30
Frequencies	1080.31	1171.44	1379.67	1421.02	1442.44
Frequencies	1529.24	3017.77	3141.77	3825.79	3827.83

C_s-Methanediol$^+$

C	0.4445874022	-0.0000336544	0.0000000000
H	1.2439140953	0.8238938235	0.0000000000
H	1.2446718009	-0.8229939815	0.0000000000
O	-0.1729491943	-0.0000287547	-1.1823993955
O	-0.1729491943	-0.0000287547	1.1823993955
H	-1.1479442620	0.0002070318	-1.1542001914
H	-1.1479442620	0.0002070318	1.1542001914

Frequencies	248.21	280.92	547.42	728.25	998.12
Frequencies	1061.71	1083.32	1129.27	1181.16	1373.14
Frequencies	1399.40	2390.95	2612.29	3664.23	3689.69

2 (CH_3OOH)

H	0.7837930584	-0.0170536630	-1.5312213358

O	-0.0511442549	-0.2767778665	-1.1179798819
O	-0.0149264634	0.5898981781	0.0586612896
C	0.0160294997	-0.2920942830	1.1712309635
H	0.0428928281	0.3643550753	2.0430678544
H	0.9108782023	-0.9200345053	1.1500421388
H	-0.8798131030	-0.9168324378	1.1962247051

Frequencies	185.63	250.43	444.01	847.56	1047.60
Frequencies	1173.35	1206.12	1361.90	1456.03	1478.74
Frequencies	1520.31	3022.61	3099.65	3126.44	3770.64

CH_3OOH^+

H	0.0196043065	0.2927208782	-1.8433893735
O	-0.0007332151	-0.3082773071	-1.0582675463
O	-0.0015346408	0.5326763593	-0.0344631165
C	-0.0003325328	-0.2306591940	1.2356775991
H	-0.2677955978	0.5239242899	1.9706495359
H	1.0197172886	-0.5992199879	1.3587644163
H	-0.7315649035	-1.0307698411	1.1344799387

Frequencies	459.80	602.98	789.46	1097.42	1114.72
Frequencies	1228.70	1430.05	1457.76	1461.75	1491.32
Frequencies	3052.45	3171.34	3209.75	3520.84	46.26

3 ($H_2CO\cdots H_2O$)

O	-0.6188089778	-0.0001369287	0.9401183954
C	0.5600010595	-0.0004327380	1.2385546784
H	0.8796163272	0.0093066488	2.2921083548
H	1.3448008851	-0.0096491105	0.4669412848
H	-0.4574858283	-0.0008353822	-1.0377826113
O	0.1174769560	0.0010560301	-1.8166475132
H	-0.4822925925	-0.0082547159	-2.5668930330

Frequencies	84.42	112.38	181.52	187.34	369.84
Frequencies	510.10	1194.17	1273.18	1529.73	1662.04
Frequencies	1750.91	2957.74	3042.99	3724.63	3895.30

$H_2CO\cdots H_2O^+$

O	-0.5980812540	0.0000000000	-0.5918991334
C	0.4653217476	0.0000000000	-1.1878430670
H	1.4165569055	0.0000000000	-0.6404216720
H	0.4153372542	0.0000000000	-2.2907571478
O	0.1631860954	0.0000000000	1.4327521978
H	-0.2367984746	0.7698155458	1.8694024145
H	-0.2367984746	-0.7698155458	1.8694024145

Frequencies	206.44	223.60	307.70
Frequencies	359.54	500.34	599.10
Frequencies	1092.06	1175.83	1398.47
Frequencies	1616.67	1716.72	2965.14
Frequencies	3088.44	3739.70	3846.74

Transition state for unimolecular dehydration of $CH_2(OH)_2$

C	0.033020	-0.017577	-0.042303
O	-0.046312	0.068312	1.624111
H	1.041980	-0.055770	1.243631
H	-0.172526	0.994098	1.886205
H	-0.415808	0.924701	-0.380781
H	-0.597855	-0.889416	-0.235157
O	1.333258	-0.152153	-0.070957

Frequencies	-1634.0402	423.8931	594.8712
Frequencies	737.2069	812.8011	1059.0533
Frequencies	1213.2433	1310.4025	1364.5278
Frequencies	1378.0252	1582.1200	2022.6064
Frequencies	3015.8874	3096.8536	3759.8827

SI References

1. B. M. Jones & R. I. Kaiser, Application of reflectron time-of-flight mass spectroscopy in the analysis of astrophysically relevant ices exposed to ionization radiation: Methane (CH_4) and D_4-methane (CD_4) as a case study. *J. Phys. Chem. Lett.* **4**, 1965-1971 (2013).
2. M. J. Abplanalp, M. Förstel, & R. I. Kaiser, Exploiting single photon vacuum ultraviolet photoionization to unravel the synthesis of complex organic molecules in interstellar ices. *Chem. Phys. Lett.* **644**, 79-98 (2016).
3. M. J. Abplanalp, S. Gozem, A. I. Krylov, C. N. Shingledecker, E. Herbst, & R. I. Kaiser, A study of interstellar aldehydes and enols as tracers of a cosmic ray-driven nonequilibrium synthesis of complex organic molecules. *P. Natl. Acad. Sci. U.S.A.* **113**, 7727-7732 (2016).
4. L. Zhou, S. Maity, M. Abplanalp, A. Turner, & R. I. Kaiser, On the radiolysis of ethylene ices by energetic electrons and implications to the extraterrestrial hydrocarbon chemistry. *Astrophys. J.* **790**, 38 (2014).
5. J. Elsila, L. J. Allamandola, & S. A. Sandford, The 2140 cm^{-1} (4.673 microns) solid CO band: the case for interstellar O_2 and N_2 and the photochemistry of nonpolar interstellar ice analogs. *Astrophys. J.* **479**, 818 (1997).
6. M. Bouilloud, N. Fray, Y. Benilan, H. Cottin, M. C. Gazeau, & A. Jolly, Bibliographic review and new measurements of the infrared band strengths of pure molecules at 25 K: H_2O, CO_2, CO, CH_4, NH_3, CH_3OH, HCOOH and H_2CO. *Mon. Not. Roy. Astron. Soc.* **451**, 2145-2160 (2015).
7. G. Socrates (2004) *Infrared and raman characteristic group frequencies* (John Wiley & Sons, Ltd., New York) 3rd Ed.
8. S. Maity, R. I. Kaiser, & B. M. Jones, Formation of complex organic molecules in methanol and methanol–carbon monoxide ices exposed to ionizing radiation – a combined FTIR and reflectron time-of-flight mass spectrometry study. *Phys. Chem. Chem. Phys.* **17**, 3081-3114 (2015).
9. C. Zhu, A. M. Turner, M. J. Abplanalp, R. I. Kaiser, B. Webb, G. Siuzdak, & R. C. Fortenberry, An interstellar synthesis of glycerol phosphates. *Astrophys. J. Lett.* **899**, L3 (2020).
10. A. M. Turner, M. J. Abplanalp, S. Y. Chen, Y. T. Chen, A. H. Chang, & R. I. Kaiser, A photoionization mass spectroscopic study on the formation of phosphanes in low temperature phosphine ices. *Phys. Chem. Chem. Phys.* **17**, 27281-27291 (2015).
11. H. Roder, The molar volume (density) of solid oxygen in equilibrium with vapor. *J. Phys. Chem. Ref. Data* **7**, 949-958 (1978).
12. D. Drouin, A. R. Couture, D. Joly, X. Tastet, V. Aimez, & R. Gauvin, CASINO V2.42 - A fast and easy-to-use modeling tool for scanning electron microscopy and microanalysis users. *Scanning* **29**, 92-101 (2007).
13. K. Raghavachari, G. W. Trucks, J. A. Pople, & M. Head-Gordon, A fifth-order perturbation comparison of electron correlation theories. *Chem. Phys. Lett.* **157**, 479-483 (1989).

14. J. M. Martin & T. J. Lee, The atomization energy and proton affinity of NH_3. An ab initio calibration study. *Chem. Phys. Lett.* **258**, 136-143 (1996).
15. R. A. Kendall, T. H. Dunning Jr, & R. J. Harrison, Electron affinities of the first-row atoms revisited. Systematic basis sets and wave functions. *J. Chem. Phys.* **96**, 6796-6806 (1992).
16. K. A. Peterson & T. H. Dunning Jr, Benchmark calculations with correlated molecular wave functions. VII. Binding energy and structure of the HF dimer. *J. Chem. Phys.* **102**, 2032-2041 (1995).
17. H. J. Werner, P. J. Knowles, G. Knizia, F. R. Manby, & M. Schütz, Molpro: a general-purpose quantum chemistry program package. *Wiley Interdiscip. Rev. Comput. Mol. Sci.* **2**, 242-253 (2012).
18. H. Werner, P. Knowles, G. Knizia, F. Manby, M. Schütz, P. Celani, W. Györffy, D. Kats, T. Korona, & R. Lindh, MOLPRO, version 2015.1, a package of ab initio programs. *University of Cardiff Chemistry Consultants (UC3): Cardiff, Wales, UK*, (2015).
19. C. Zhu, R. Frigge, A. Bergantini, R. C. Fortenberry, & R. I. Kaiser, Untangling the formation of methoxymethanol (CH_3OCH_2OH) and dimethyl peroxide (CH_3OOCH_3) in star-forming regions. *Astrophys. J.* **881**, 156 (2019).
20. R. Spence & W. Wild, The thermal reaction between chlorine and formaldehyde. *J. Am. Chem. Soc.* **57**, 1145-1146 (1935).